PHOTODEGRADATION OF RhB UNDER VISIBLE LIGHT BY PT/TIO$_2$ NANOPARTICLES PREPARED THROUGH PHOTOREDUCTIVE DEPOSITION PROCESS

Jianye Li[a,b,#], **Youjun Yan**[b,*,iD], **Guangjin Sun**[b,c], **Jianwei Yang**[b], **Zhixiao Wang**[b] and **Xue Yan**[b]

[a]Shandong Peninsula Engineering Research Center of Comprehensive Brine Utilization, Weifang University of Science and Technology, 262700, Weifang, Shandong, China
[b]Shandong Moris Environmental Industry Co., LTD, 262714, Weifang, Shandong, China
[c]Ocean University of China, 266100, Qingdao, Shandong, China

Pt/TiO$_2$ nanoparticles were prepared by a simple two-step aqueous solution method, which consists of a low temperature hydrothermal step and a photoreduction deposition step. The as-prepared samples were characterized by XRD, TEM, XPS, UV-vis, and BET techniques. The as-prepared samples exhibited enhanced photocatalytic activity towards the degradation of rhodamine B (RhB) under visible light irradiation. With increasing Pt content from 0.25 to 1 wt.%, the band gap energies shift from 2.32 to 1.64 eV. The 0.75 wt.% Pt/TiO$_2$ sample showed the best photocatalytic activity, which could be ascribed to the formation of a Schottky barrier and the localized surface plasmon resonance effect of Pt nanoparticles. And the as-prepared samples also displayed excellent stability and reusability in multiple experimental cycles.

Keywords: RhB; visible light; nano-Pt/TiO$_2$; photoreductive.

INTRODUCTION

TiO$_2$ has become one of the most promising green catalysts due to its stable chemical properties, high catalytic activity and low selectivity for organic degradation.[1-6] However, the wide band gap of pure TiO$_2$ (3.2 ev) limits its visible light utilization. At the same time, the low quantum efficiency and high recombination rate of photocarriers limit the industrial application of TiO$_2$ photocatalytic technology. Therefore, how to improve the quantum efficiency, effective separation of photocarriers, the utilization of incident light, and the response range of visible light are the bottlenecks of the development of photocatalysis technology and have become the research hotspot in the field.[7-11]

Awazu *et al.* proposed the concept of surface plasma photocatalytic materials and prepared the Ag/TiO$_2$ photocatalyst with surface plasmon resonance effect for the first time in 2008.[12] The as-prepared photocatalyst showed high visible light photocatalytic activity because of the localized surface plasmon resonance (SPR) of Ag nanoparticles. Meanwhile, the noble metal nanoparticles can effectively capture photogenerated electrons, promote the separation of photogenerated electrons and holes, and improve photocatalytic efficiency. Since then, as a new type of visible light response photocatalyst, plasma photocatalyst has been favored by researchers.[13-19]

In this work, highly dispersed nano-TiO$_2$ aqueous dispersion was prepared by the hydrothermal method. With the dispersion as the precursor, the nano Pt/TiO$_2$ catalyst was prepared by photochemical reduction deposition. The composition, crystal form, and micromorphology of the catalyst were characterized. The as-prepared Pt/TiO$_2$ catalyst showed excellent photocatalytic performance and stability in the degradations of RhB under visible light irradiation.

EXPERIMENTAL

Preparation of the Nano-TiO$_2$ aqueous Dispersion

Ti(SO$_4$)$_2$ (AR, Sinopharm Chemical Reagent Co. Ltd), CO(NH$_2$)$_2$ (AR, Sinopharm Chemical Reagent Co. Ltd), and distilled water were used to prepared nano-TiO$_2$ aqueous dispersion.

The nano-TiO$_2$ aqueous dispersion was prepared by a hydrothermal condition. Firstly, 7.2 g of Ti(SO$_4$)$_2$ were dissolved in 300 mL distilled water by ultrasound dispersion. After about 10 min, the Ti(SO$_4$)$_2$ solution was obtained. Meanwhile, 2.7 g of CO(NH$_2$)$_2$ were dissolved in 100 mL distilled water by the same method. Then, CO(NH$_2$)$_2$ solution was added into Ti(SO$_4$)$_2$ solution drop by drop with vigorous stirring. After stirring for about 30 min, a transparent solution was obtained, which was then transferred into Teflon-lined stainless-steel autoclaves and reacted at a given temperature for 24 h, and then cooled naturally. The precipitate was collected by centrifugation and washed with distilled water until the conductivity of the residue solutions no longer changed. Lastly, the as-prepared nano-TiO$_2$ was dispersed in distilled water by ultrasound dispersion.

Synthesis of Pt/TiO$_2$ catalysts

Pt/TiO$_2$ catalysts were prepared by photochemical deposition. And H$_2$PtCl$_6$ was used as a starting material. Firstly, 200 mL of isopropanol and 200 mL of distilled water were mixed evenly and then transferred to the photocatalytic reaction bottle. Nano-TiO$_2$ dispersion was dropped into the mixed solution slowly. Sealed the reaction bottle, and argon gas was used as the protective gas. 0.5 mol L^{-1} of H$_2$PtCl$_6$ was added into the isopropanol aqueous solution drop by drop slowly under magnetic stirring and UV irradiation. Two hours later, the precipitate was collected by centrifugation and washed with distilled water. The as-prepared Pt/TiO$_2$ catalysts were dispersed in distilled water by ultrasound dispersion.

*e-mail: wkyyyj@163.com
#alternative e-mail: ljy@techmoris.com

Characterization

Phase structures of all samples were identified by powder X-ray diffraction at room temperature on a Rigaku Dmax 2500 PC apparatus (copper target, $K\alpha$, $\lambda = 0.15418$ nm). The surface areas of the samples were determined by N_2 adsorption using the Brunauer–Emmett–Teller (BET) method with a Micromeritics ASAP 2020 plus instrument (America) at the temperature of liquid nitrogen. All of the samples were degassed at 150 °C under vacuum for 12 h and finally outgassed to 10^{-3} Torr.

The particle size and the composite structure were measured with high resolution transmission electron microscope (Tecnai G2 T20, FEI, America). The X-ray photoelectron spectroscopy (XPS) measurement was performed using a K-Alpha+ XPS spectrometer (220i-XL, VG, UK). The optical absorbance properties of the as-prepared samples were measured by diffuse reflectance spectroscopy (U-3900, Hitachi, Japan) at room temperature.

Photocatalytic degradation of RhB

The photocatalytic activity of each sample was estimated by measuring the decomposition rate of rhodamine B (RhB) under visible light irradiation. A 50 W xenon lamp with a peak wavelength of 420 nm was used as a light source. The reaction suspension was prepared by adding the required amount of Pt/TiO$_2$ into 200 mL of RhB solutions (9 mg L^{-1}). Before illumination, the solution was stirred for 1 h in dark to reach an absorption-desorption equilibrium of RhB. Subsequently, the suspension containing RhB and Pt/TiO$_2$ was irradiated with constant stirring. 5 mL of the suspensions were collected every 60 min, centrifuged, and filtered. The UV-vis absorption spectra of the supernatant were measured using a UV-vis spectrophotometer (DR3900).

RESULTS AND DISCUSSION

Characterization of the catalysts

Figure 1 shows the X-ray diffraction patterns of the as-prepared samples with different amounts of Pt. By comparing with JCPDS card of anatase (No. 21–1272), rutile (No. 65–0190) and Pt (No. 88-2343), it could be observed that the diffraction peaks at a diffraction angle of 25.28°correspond to the (101) crystal surface of anatase TiO$_2$. And the diffraction peaks at diffraction angles of 27.45°, 36.00°, 54.26° correspond to the (110), (101), (221) crystal surfaces of rutile TiO$_2$ respectively. It confirms that the coexistence of anatase and rutile. There is no diffraction peak of Pt ($2\theta = 39.8°$) in the XRD patterns, which may be due to the low concentration of Pt on the surface and no obvious crystal phase effect.

The average crystallite sizes of both anatase and rutile were calculated from the full width at half maximum of XRD peaks by using the Scherrer formula separately.

$$D = K\lambda/(\beta\cos\theta) \quad (1)$$

where λ is the wavelength of the incident X-ray (nm), β is the full width at half maximum value of the XRD diffraction lines (nm), θ is the angle of diffraction, and K=0.89.

Table 1 shows the average crystallite sizes of both anatase and rutile nanoparticles in the as-prepared samples. It can be seen from Table 1 that the crystallite sizes of the as-prepared samples are about 19-30 nm.

The amount of anatase and rutile phase is 79.22% and 20.78%, respectively, calculated from the intensities of two peaks: (101) and (110) plane by using Equation (2).
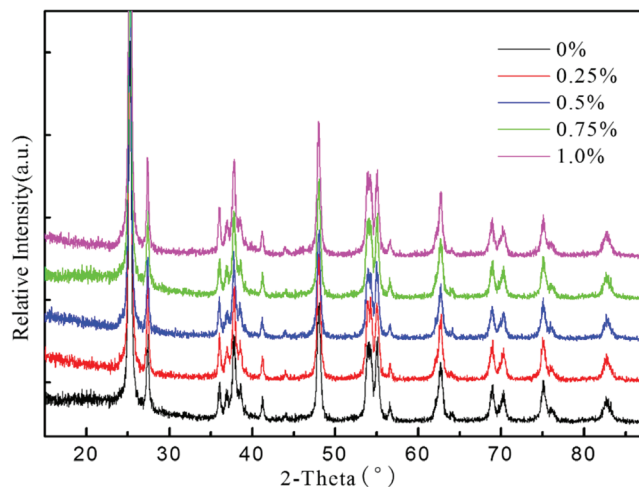
Figure 1. XRD patterns of Pt/TiO$_2$ catalysts

Table 1. The crystallite size of both anatase and rutile nanoparticles

Samples	D(anatase)/nm	D(rutile)/nm
TiO$_2$	19.82	24.12
0. 25 wt.% Pt/TiO$_2$	20.05	29.39
0.50 wt.% Pt/TiO$_2$	19.88	27.56
0.75 wt.% Pt/TiO$_2$	19.82	24.12
1.00 wt.% Pt/TiO$_2$	19.94	27.22

$$X_A(\%) = 100/(1+1.265 I_R/I_A) \quad (2)$$

where X_A represents the relative weight percentage of rutile; I_A represents the X-ray integrated intensities of the (101) diffraction of anatase and I_R is the integrated intensities of the (110) diffraction of rutile.

The TEM images of the sample 0.75 wt.% of Pt/TiO$_2$ are shown in Figure 2. The images show that most of the prepared TiO$_2$ nanoparticles are with an average size of 20-30 nm. The particle sizes agree well with the crystallite sizes calculated with the Scherrer formula. It also can be seen from the images that the as-prepared Pt nanocrystals uniformly distributed on the surface of the composites, which have an average diameter of about 3-7 nm. The HRTEM images in Figure 2c display two types of lattice fringes with spacings of 0.326 nm and 0.221 nm, which belong to anatase (110) plane and cubic Pt (111) plane respectively. This further proves the existence of the cubic Pt.

XPS analysis was carried out to investigate the surface chemical states of the as-prepared samples. The surface XPS spectra of the sample 0.75 wt.% Pt/TiO$_2$ are shown in Figure 3. It can be seen that there are only Pt, Ti, and O related peaks, indicating the high purity of the as-prepared Pt/TiO$_2$. Figure 3a shows the high-resolution XPS spectrum of the Pt 4f peak for the sample. As seen from Figure 3a, Pt/TiO$_2$ exhibits a Pt 4f signal that can be deconvoluted into two pairs of doublets. The two strong peaks located at 70.59 (Pt 4f$_{7/2}$) and 74.05 eV (Pt 4f$_{5/2}$) are attributed to metallic Pt.[20-22] And the other weaker peaks at 71.3 and 75.4 eV are assigned to Pt 4f$_{7/2}$ and Pt 4f$_{5/2}$ of Pt (II). It was found that 71.2% of Pt was in the metallic state and 28.8% in the form of Pt (II) which might form during transfer of the sample in the air to the XPS chamber.[23,24]

Figure 3b shows the high-resolution XPS spectrum of the Ti 4p peak for the sample 0.75 wt.% of Pt/TiO$_2$. It can be seen that there are two symmetry peaks at 458.79 eV and 464.48 eV at the spectrum, which belong to Ti 2p$_{3/2}$ and 2p$_{1/2}$ respectively. These are
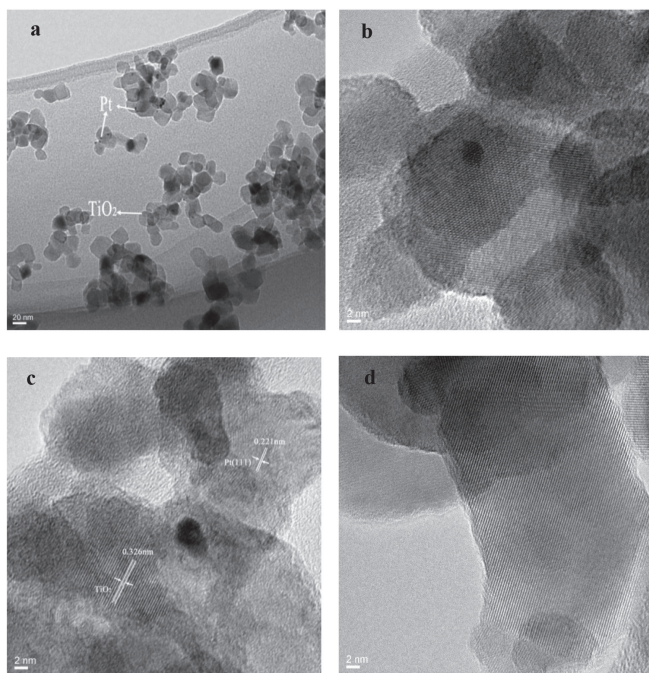
***Figure 2.** TEM (a) and HRTEM (b-d) images of the as-prepared Pt/TiO₂ catalysts*

the characteristic peaks for Ti^{4+} in TiO_2. The peak around at 530 eV in the XPS spectrum (Figure 3c) corresponds to the Ti-O bond in TiO_2.[25]

Nitrogen adsorption-desorption isotherm plot and pore size distribution of the as-prepared sample of 0.75 wt.% Pt/TiO₂ are illustrated in Figure 4. The sample exhibits typical type VI adsorption-desorption isotherm. The as-prepared sample mostly contains mesoporous with diameters in the range of 10-50 nm. And a few pore diameters (50 nm) are larger than the particle size (20-30 nm by TEM), which indicates that the as-prepared sample has a certain agglomeration phenomenon.

The specific surface areas of the samples evaluated via the Brunauer-Emmett-Teller (BET) method were listed in Table 2. It can be seen from the table that the specific surface area of the sample decreases with the increase of Pt-loading. This may be caused by the deposition of Pt nanoparticles, which blocked some pores that result in a smaller surface area.[26]

The optical properties of as-prepared Pt/TiO₂ nanoparticles were studied using a UV-visible spectroscope. Figure 5a shows UV-vis DRS of the as-prepared Pt/TiO₂ composites. It reveals that Pt/TiO₂ composites have strong absorptions in the visible light region, which is confirmed by the deepening of the apparent color of the as-prepared

Pt/TiO₂ composites. The red shift of the absorption band edge was observed with the increase of deposited Pt for the as-prepared samples (Figure 5a). The band gap energies of the as-prepared samples were assessed through the plotting of $(\alpha h\nu)^{1/2}$ vs. $h\nu$.[27] As shown in Figure 5b, with increasing Pt content from 0.25 to 1 wt.%, the band gap energies shift from 2.32 to 1.64 eV.

Photocatalytic activity

Photocatalytic degradation of RhB was carried out to test the photocatalytic activity of the as-prepared samples under the irradiation of visible light. The factors affecting the photocatalytic performance and cycle life of nanocomposites were also investigated. Besides, blank experiments with and without pure TiO₂ nanoparticles were also carried out for comparison.

Effect of the amount of deposited Pt

Figure 6 shows the photodegradation rate of RhB under visible light irradiation with 500 mg L^{-1} different samples. It can be seen from Figure 6 that pure TiO₂ showed poor photocatalytic activity. The as-prepared Pt/TiO₂ catalysts exhibited significantly better activity than pure TiO₂. The enhanced photocatalytic activity of the as-prepared composites photocatalysts under visible light can be attributed to the deposition of Pt nanoparticles, which show significant localized surface plasmon resonance effect,[28] which makes Pt/TiO₂ have strong absorption in the visible light area, and promotes the formation of photogenerated electrons and holes in the nanocatalyst under the visible light irradiation. On the other hand, deposited Pt nanoparticles can promote separating efficiency of surface photo-induced current carriers and decrease the electron-hole recombination.

In addition, because the Fermi energy level of semiconductor TiO₂ is higher than that of Pt nanoparticles, the photogenerated electrons will transfer from the conduction band of TiO₂ to the surface of Pt nanoparticles until both sides have the same Fermi energy level. At the same time, due to the transfer of photogenerated electrons, the energy band of TiO₂ will bend upward at the interface of Pt and TiO₂, forming Schottky barrier,[29,30] which will further inhibit the recombination of photogenerated carriers. The quantum yield and photocatalytic efficiency are improved.

The photodegradation rate improved with the increase of the depositing Pt (Figure 6). The improved photodegradation rate may be caused by the higher visible light absorption on the as-prepared Pt/TiO₂ catalysts, which is consistent with UV-vis analysis. The sample deposited with 0.75 wt.% Pt nanoparticles shows the maximum visible light photoactivity. When the Pt content was higher than 0.75 wt.%, the degradation rate of RhB declined. Because a large of Pt nanoparticles cover the surface of TiO₂ and occupy
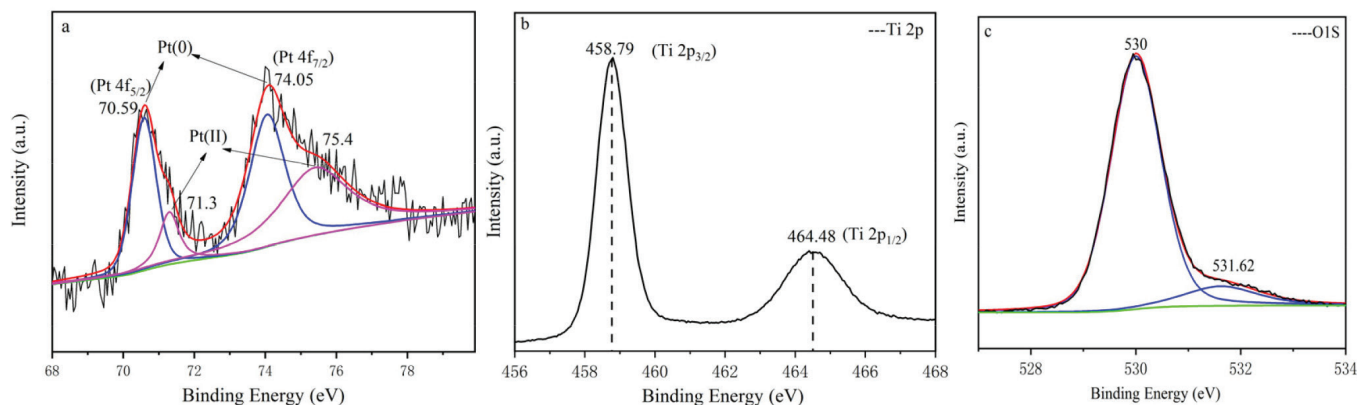
***Figure 3.** XPS spectra of Pt/TiO₂ catalysts:(a) Pt 4f, (b) Ti 2p, (c) O 1s*
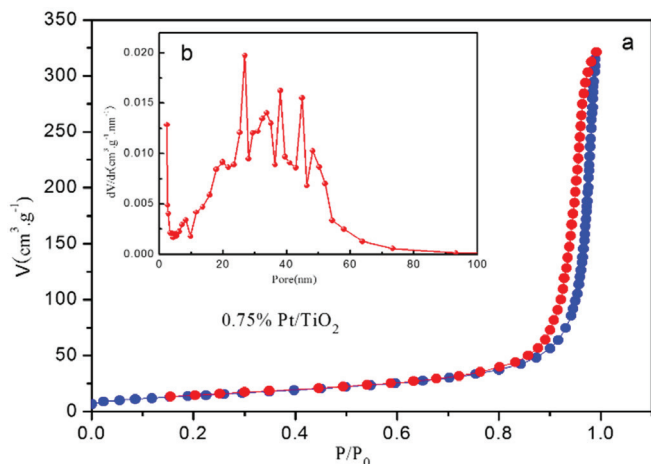
Figure 4. *(a) N$_2$ adsorption-desorption isotherm plot and (b) pore size distribution of the as-synthesized samples: 0.75 wt.% Pt/TiO$_2$*

Table 2. The BET specific area of Pt/TiO$_2$

Catalyst	S_{BET} /m^2 g^{-1}
TiO$_2$	54.25
0. 25 wt.% Pt/TiO$_2$	49.47
0.50 wt.% Pt/TiO$_2$	48.13
0.75 wt.% Pt/TiO$_2$	48.06
1.00 wt.% Pt/TiO$_2$	47.88

more active sites, which hinders the contact between TiO$_2$ and RhB, reduces the specific surface area, and reduces the efficiency of the photocatalysts. At the same time, excessive nano Pt deposition on the surface of TiO$_2$ catalyst can bridge the band gap and act as electron–hole recombination centers, which will increase electron–hole recombination,[31] lead to the decrease of photoactivity of the as-prepared samples eventually.

Furthermore, the deposited Pt nanoparticles will agglomerate when the deposition amount of Pt nanoparticles is too large. The agglomerated Pt will become electron - hole recombination center, and the activity of the photocatalyst will decline. Therefore, it is necessary to determine the optimal Pt deposition to prepare high activity Pt/TiO$_2$ photocatalyst.

Effect of the amount of Pt/TiO$_2$

It's well known that, the dosage of photocatalyst is also an important factor affecting photodegradation efficiency. The influence of the amount of 0.75 wt.% Pt/TiO$_2$ catalyst on the photocatalytic activity of RhB was also investigated (Figure 7). Compared with the sample synthesized with Ti(OBu)$_4$ as the precursor through the sol-gel method, the as-prepared showed higher BET surface area and more photodegradation efficiency.

It can be seen from Figure 7 that with the increase of catalyst dosage from 250 to 500 mg L^{-1}, the degradation rate of RhB increases gradually. However, when the catalyst dosage increased to 500 mg L^{-1}, the degradation efficiency of RhB is the highest. Further increasing the amount of the as-prepared 0.75 wt.% Pt/TiO$_2$ photocatalyst did not result in further increase of degradation efficiency of RhB. It's easily understood that the lower of the catalyst concentration, the lower the utilization visible light, and the degradation rate is lower also. With the increase of catalyst concentration, the utilization of visible light is increased, so the reaction rate is accelerated. While when the Pt/TiO$_2$ photocatalyst concentration is too large, the excessive amount of photocatalysts will reduce the light transmittance. So, the photocatalytic reaction speed will be slowed down with increasing the amount of catalyst.

Stability of the photocatalyst

The stability and reusability of photocatalyst are also important for its industrial application. The stability of the as-prepared Pt/TiO$_2$ photocatalyst was investigated by photodegrading RhB under visible light irradiation. In this study, RhB was added to the reaction system continuously, which involved 500 mg L^{-1} Pt/TiO$_2$ photocatalyst and 9 mg L^{-1} RhB. After 5 hours of reaction, the second addition of RhB was added to restore the RhB concentration to 9 mg L^{-1}. As shown in Figure 8, the degradation rate of RhB in the second cycle is almost the same as that in the first cycle. The degradation rate of RhB does not show a significant decline after 9 cycles, which fully proves that the as-prepared Pt/TiO$_2$ has a stable visible photocatalytic performance.

CONCLUSIONS

Nano-TiO$_2$ aqueous dispersion was synthesized by hydrothermal method, and Pt nanoparticles were deposited on the surface of the as-prepared nano-TiO$_2$ by photochemical reduction method. The composite catalyst was characterized by XRD, XPS, TEM, etc. It
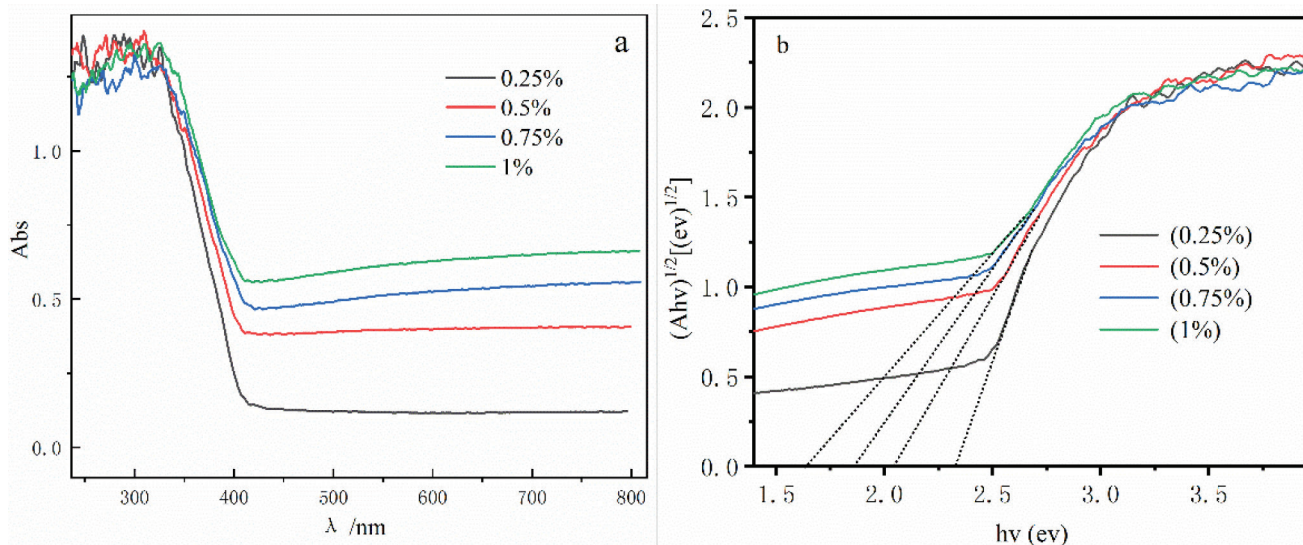
Figure 5. *(a) UV-vis spectra of Pt/TiO$_2$ catalysts; (b) the plotting of (Ahv)$^{1/2}$ vs. hv*
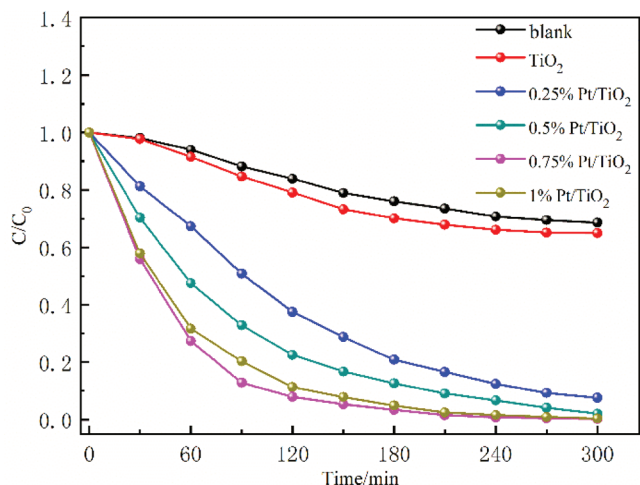
Figure 6. *The influence of Pt loads on catalytic performance*
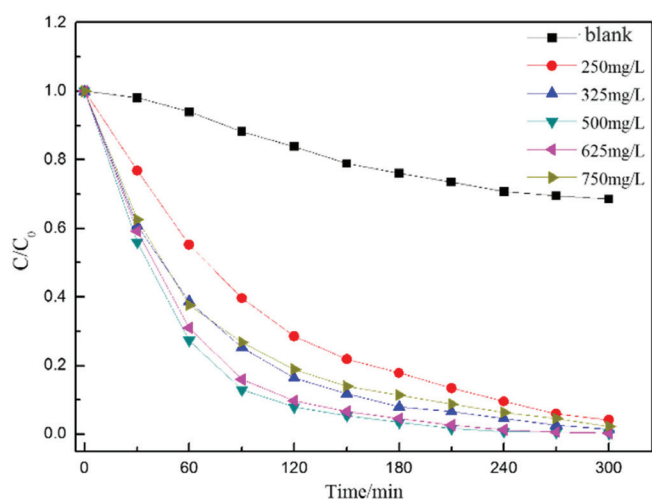
Figure 7. *The relationship between the catalyst dosage and the removal degree*
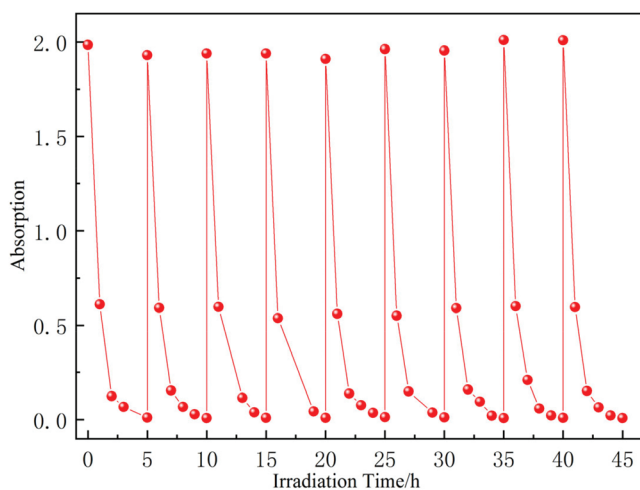
Figure 8. *The RhB degradation durability test of Pt/TiO$_2$*

was found that Pt (0) nanoparticles were uniformly dispersed on the surface of TiO$_2$, the particle sizes of the as-prepared TiO$_2$ nanoparticles were in the range of 19-30 nm, and the crystalline form of TiO$_2$ was mainly anatase and rutile. Due to the effect of plasma resonance, the absorption edge band of TiO$_2$ photocatalyst showed red shift. And the deposition of nano Pt effectively enhances the separation

and transfer efficiency of photogenerated electrons, hinders the recombination of photogenerated carriers, and effectively improves the photocatalytic performance. The photodegradation activity of the as-prepared Pt/TiO$_2$ photocatalysts were investigated by depredating RhB under simulated visible light irradiation. The sample of 0.75 wt.% Pt/TiO$_2$ showed the best photodegradation efficiency and the best catalyst dosage is 500 mg L^{-1}. The as-prepared Pt/TiO$_2$ exhibited high photocatalytic stability and maintain good photocatalytic activity after nine cycles.

ACKNOWLEDGEMENTS

REFERENCES

1. Tong, H.; Ouyang, S.; Bi, Y.; Umezawa, N.; Oshikiri, M.; Ye, J.; *Adv. Mater.* **2012**, *24*, 229.
2. Fujishima, A.; Honda, K.; *Nature* **1972**, *238*, 37.
3. He, D. Y.; Yang, Y.; Tang, J. J.; Zhou, K. G.; Chen, W.; Chen Y. Q.; Dong, Z. J.; *Environ. Sci. Pollut. Res. Int.* **2019**, *45*, 43.
4. Zhang, P. H.; Li, Y. C.; Zhang, X. L.; Hu, H. B.; Wang, J. S.; *Technol. Water Treat.* **2019**, *45*, 52.
5. Sacco, O.; Vaiano V.; Daniel C.; Navarra, W.; Venditto, V.; *Mater. Sci. Semicond. Process.* **2018**, *80*, 104.
6. Zhao, Q.; Wang, M.; Yang, H.; Shi, D.; Wang, Y. Z.; *Ceram. Int.* **2018**, *44*, 5145.
7. Wu, L. L.; Shi, S.; Li, Q. D.; Zhang, X. Y.; Cui, X. L.; *Int. J. Hydrogen Energy* **2019**, *44*, 720.
8. Liu, R. D.; Li, H.; Duan, L. B.; Shen, H.; Zhang, Y. Y.; Zhao X. R.; *Ceram. Int.* **2017**, *43*, 8648.
9. Trevisan, V.; Olivo, A.; Pinna, F.; *Appl. Catal., B* **2014**, *160*, 152.
10. Yan, X.; Xing, Z.; Cao, Y.; Hu, M. Q.; Li, Z. Z.; Wu, X. Y.; Zhu, Q.; Yang, S. L.; Zhou, W.; *Appl. Catal., B* **2017**, *219*, 572.
11. Police, A. K. R.; Vattikuti, S. V. P.; Mandari, K. K.; Chennaiahgari, M.; Phanikrishna, S. M. V.; Valluri, D.; K.; Byon, C.; *Ceram. Int.* **2018**, *44*, 11783.
12. Awazu, K.; Fujimaki, M.; Rockstuhl, C. A.; *J. Am. Chem. Soc.* **2008**, *130*, 1676.
13. Wang, L. M.; Yao, B. H.; Pei, L.; *Chin. J. Environ. Eng.* **2014**, *12*, 5289.
14. Kuo, D.; Hsu, W.; Yang, Y.; *Appl. Catal., B* **2016**, *184*, 191.
15. Yurdakal, S.; Tek, B. S.; Degirmenci, C.; Palmisano, G.; *Catal. Today* **2017**, *281*, 53.
16. Deng, X. Q.; Liu, J. L.; Li, X. S.; Zhu, B.; Zhu X. B.; Zhu, A. M.; *Catal. Today* **2017**, *281*, 630.
17. Jiao, Y. Z.; Yang, X.; Deng, Z. F.; Tian, Y.; *Environ. Chem.* **2011**, *5*, 970.
18. Moslah, C.; Kandyla, M.; Mousdis, G. A.; Petropoulou, G.; Ksibi, M.; *Phys. Status Solidi A* **2018**, *215*, 1800023.
19. Xu, G. Q.; Liu, H. P.; Wang, J. W.; Lv, J.; Zheng, Z. X.; Wu, Y. C.; *Electrochim. Acta* **2014**, *121*, 194.
20. Yang, J. C.; Kim, Y. C.; Shul, Y. G.; Shin, C. H.; Lee, T. K.; *Appl. Surf. Sci.* **1997**, *121*, 525.
21. Cho, K.; C.; Hwang, K. C.; Sano, T.; Takeuchi, K.; Matsuzawa, S.; *J. Photochem. Photobiol., A* **2004**, *161*, 155.
22. Pitchon, V.; Fritz, A.; *J. Catal.* **1999**, *186*, 64.
23. Nie, R.; Wang, J.; Wang, L.; Qin, Y.; Chen, P.; Hou, Z.; *Carbon* **2012**, *50*, 586.
24. Kim, J. H.; Choi, S. M.; Nam, S. H.; Seo, M. H.; Choi, S. H.; Kim, W. B.; *Appl. Catal., B* **2008**, *82*, 89.

25. Fu, P. F.; Zhang, P. Y.; *Chin. J. Catal.* **2014**, *35*, 210.
26. An, M.; Li, L.; Tian, Y.; Yu, H.; Zhou, Q.; *RSC Adv.* **2018**, *8*, 18870.
27. Li, L.; Zhang, X. L.; Zhang, W. Z.; Wang, L. L.; Chen, X.; Yu, Gao.; *Colloids Surf., A* **2014**, *457*, 134.
28. Zhang, F. F.; Liu, W.; Liu, Y. S.; Wang, J. Y.; Ji, G. B.; *J. Nanopart. Res.* **2015**, *17*, 62.

29. Hufschmidt, D.; Bahnemann, D.; Testa, J. J.; Emilio, C. A.; Litter, M. I.; *J. Photochem. Photobiol., A* **2002**, *148*, 223.
30. Filippo, E.; Carlucci, C.; Capodilupo, A. L.; Perulli, P.; Conciauro, F.; Corrente, G. A.; Gigli, G.; Ciccarella, G.; *Mat. Res.* **2015**, *18*, 473.
31. Christopher, L. M.; Zhou, Y.; Aaron, M. H.; Alan, W. W.; Charles, B. M.; *J. Phys. Chem. C* **2012**, *116*, 10138.